Atmos. Meas. Tech., 17, 1837–1850, 2024
https://doi.org/10.5194/amt-17-1837-2024

Atmospheric Measurement Techniques
Open Access
EGU

Directly measuring the power-law exponent and kinetic energy of atmospheric turbulence using coherent Doppler wind lidar

Jinhong Xian[1,2], Chao Lu[2], Xiaoling Lin[2], Honglong Yang[2], Ning Zhang[1,3], and Li Zhang[2]

[1]School of Atmospheric Sciences, Nanjing University, Nanjing 210023, China
[2]Shenzhen National Climate Observatory, Meteorological Bureau of Shenzhen Municipality, Shenzhen 518040, China
[3]Key Laboratory of Urban Meteorology, China Meteorological Administration, Beijing 100089, China

Correspondence: Honglong Yang (yanghonglong@weather.sz.gov.cn) and Ning Zhang (ningzhang@nju.edu.cn)

Received: 1 December 2023 – Discussion started: 11 December 2023
Revised: 30 January 2024 – Accepted: 23 February 2024 – Published: 2 April 2024

Abstract. Atmospheric turbulence parameters, such as turbulent kinetic energy and dissipation rate, are of great significance in weather prediction, meteorological disasters, and forecasting. Due to the lack of ideal direct detection methods, traditional structure function methods are mainly based on Kolmogorov's assumption of local isotropic turbulence and the well-known $-5/3$ power law within the inertial subrange, which limits their application. Here, we propose a method for directly measuring atmospheric turbulence parameters using coherent Doppler wind lidar, which can directly obtain atmospheric turbulence parameters and vertical structural features, breaking the limitations of traditional methods. The first published spatiotemporal distribution map of the power-law exponent of the inertial subrange is provided in this study, which indicates the heterogeneity of atmospheric turbulence at different altitudes and also indicates that the power-law exponent at high altitudes does not fully comply with the $-5/3$ power law, proving the superiority of our method. We analyze the results under different weather conditions, indicating that the method still holds. The turbulent kinetic energy and power-law index obtained by this method are continuously compared with the results obtained with an ultrasonic anemometer for a month-long period. The results of the two have high consistency and correlation, verifying the accuracy and applicability of the proposed method. The proposed method has great significance in studying the vertical structural characteristics of atmospheric turbulence.

1 Introduction

Turbulence is the main form of motion in the atmospheric boundary layer. It plays a major role in the transportation and exchange of momentum, heat, water vapor, and matter between the surface of the Earth and the atmosphere, directly affecting human life and production activities and playing a crucial role in atmospheric motion and weather evolution (Byzova et al., 1989; Stull, 1988; Gottschall and Peinke, 2008). At present, there are still many difficulties related to the study of turbulence, and addressing them requires improvements in observational technology. Therefore, the development of atmospheric turbulence detection technology can strengthen our understanding of atmospheric turbulent motion and accelerate the development of atmospheric turbulence theory. In atmospheric modeling in particular, it is of great significance to obtain the relevant parameters and structural characteristics of atmospheric turbulence (Banakh and Smalikho, 2013).

In the past, there were few detection methods for measuring or inferring low-level turbulence parameters, mainly through the installation of three-dimensional ultrasonic anemometers in meteorological gradient towers (Sathe and Mann, 2013). The detection height, density, and detection ability of the detectors were limited, which hindered the development of boundary layer turbulence theory. Fortunately, with the development of remote sensing technology, as an active remote sensing device with fast response speed and three-dimensional scanning ability, coherent Doppler wind lidar has gradually become the main means of obtaining low-level atmospheric turbulence intensity (Mann et al., 2010;

Choukulkar et al., 2017; Bonin et al., 2017, 2016; Jin et al., 2022; Smalikho et al., 2005; Branlard et al., 2013; Banakh et al., 2021; O'Connor et al., 2010).

According to Kolmogorov's theory of local homogeneity and isotropy, the structure function can only be determined by the kinetic energy dissipation rate (Kolmogorov, 1941; Kolmogorov, 1991). Therefore, the structure function can be calculated based on the wind speed fluctuation term, and the kinetic energy dissipation rate can in turn be estimated based on the relationship between the structure function and the kinetic energy dissipation rate given by a statistical turbulence model (Sathe and Mann, 2013). It is called the structure function method, which is an indirect method. Based on this principle, researchers have proposed different acquisition methods. In 2002, Frehlich and Cornman obtained the spatial statistical characteristics of a simulated turbulent velocity field using radial velocity estimation from coherent Doppler lidar data and subsequently calculated the turbulent energy dissipation rate (Frehlich and Cornman, 2002). In 2005, Smalikho et al. (2005) used coherent wind lidar to invert atmospheric turbulence parameters with two methods, i.e., the Doppler spectral width and height structure function, using the range height indicator (RHI) scanning mode. The experimental results were numerically simulated, which confirmed the reliability of these two methods (Smalikho et al., 2005). In 2008, Frehlich and Kelley obtained turbulence parameters in the boundary layer using longitudinal and transverse structure function methods in the plane position indicator (PPI) scanning mode with fixed pitch angle and changing azimuth angle (Frehlich and Kelley, 2008). The inversion results were compared with the detection results of ultrasonic anemometers, and the data consistency was good. In 2012, Chan and Lee divided radial wind field data into subsectors under the PPI scanning mode and calculated the turbulence dissipation rate within each subsector using velocity structure functions, thus obtaining the spatial distribution of the turbulence dissipation rate (Chan and Lee, 2012). In 2017, Smalikho and Banakh used the azimuth structure function in the velocity azimuth display (VAD) scanning mode to invert atmospheric turbulence parameters and extended the applicability of this method from the convective boundary layer to the stable boundary layer (Smalikho and Banakh, 2017). From 2017 to 2019, Zhai et al. (2017) studied the vertical structure characteristics of turbulence in the atmospheric boundary layer using various lidar observation models such as the VAD, PPI, and RHI (Zhai et al., 2017). They analyzed interaction characteristics between a wind turbine wake and atmospheric turbulence under the influence of underlying surfaces with different roughness and explored the influence of atmospheric turbulence on the evolution process of aircraft wake vortices. In 2023, Wang et al. (2023) used shipborne coherent Doppler lidar to measure the energy dissipation rate and wind shear intensity of turbulent flows at sea based on the structure function method, achieving the classification of turbulent mixing sources (Wang et al., 2023). These previous studies are based on the indirect acquisition of atmospheric turbulence parameters using a structure function, which in turn relies on the assumptions of isotropy and a power-law exponent of $-5/3$.

Due to the extremely complex turbulence in the atmospheric boundary layer, the assumptions of isotropy and the $-5/3$ power law are more realistic in the near-surface layer of the atmosphere but may not fully hold true in some complex terrains or high altitudes. Panofsky et al. (1982) specifically observed various turbulence structures under complex terrain conditions and found that different terrain conditions have different turbulence energy spectral characteristics (Panofsky et al., 1982). The study by Chellali et al. (2010) also indicates that the characteristics of turbulent energy spectra are influenced by factors such as terrain and spatial location (Chellali et al., 2010). The current methods of measuring atmospheric turbulence parameters using wind lidar data based on Kolmogorov's assumption of local isotropic turbulence and the well-known $-5/3$ power law are indirect, which have limited applicability and cannot produce accurate turbulence processes. Therefore, the aim of this study is to find a more direct method for obtaining atmospheric turbulence parameters from the perspective of spectral analysis, without the assumptions of local isotropic turbulence and the $-5/3$ power law. In Sect. 2, we introduce the instruments and data quality control methods. In Sect. 3, we present the obtained turbulence spectra and propose a method for directly obtaining atmospheric turbulence parameters using coherent Doppler wind lidar data. On this basis, we study the vertical characteristics of atmospheric turbulence obtained from wind lidar data and compare them with the results from three-dimensional ultrasonic anemometers to verify their accuracy, as shown in Sect. 4. The main conclusions of this study are presented in Sect. 5.

2 Instruments and data quality control

The Shenzhen Shiyan Observation Base (22.65562° N, 113.90586° E) has a 356 m high meteorological gradient observation tower, which is the tallest in Asia (Zhou et al., 2023). The surrounding terrain and landforms of the observation tower are shown in Fig. 1a, and b shows the wind lidar instrument beneath the gradient observation tower. Four three-dimensional ultrasonic anemometers (CSAT3, Campbell Scientific, Utah, USA) are installed at heights of 10, 40, 160, and 320 m on the gradient observation tower. From Fig. 1, it can be seen that there are no large obstacles (such as tall buildings) around the tower. Located 1–2 km northeast of the tower there is farmland, while tall buildings are located in distant suburbs. The terrain to the south and northwest of the gradient tower is generally flat, almost completely covered by forests and lakes. Due to its excellent geographical location with no obstructions around it, the monitored data are highly representative. We used wind lidar data and data

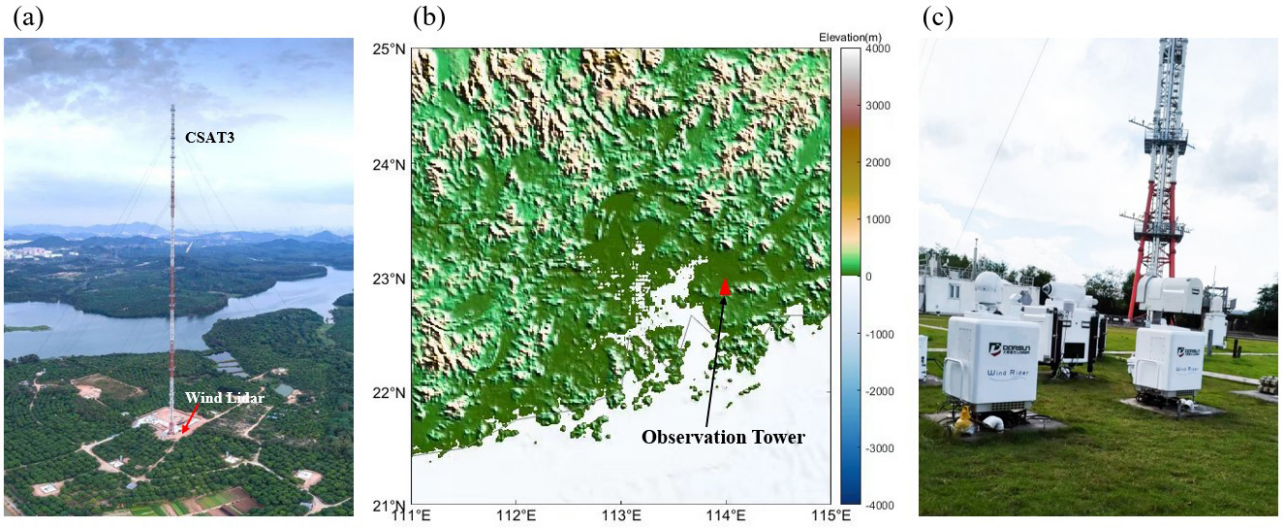

Figure 1. Layout diagram **(a)**, topographic map **(b)** of the surrounding area of the meteorological gradient observation tower, and installation diagram of the wind lidar below the tower **(c)**.

obtained with the three-dimensional ultrasonic anemometer in this study. The observational frequency of the ultrasonic anemometer is 10 Hz, and the wind speed accuracy can reach 0.1 m s^{-1}. The wind lidar (DSL-W, Darsunlaser Technology Co., Ltd., Shenzhen, China) detects a blind spot of 30 m, with a maximum detection height of 3 km and a vertical resolution of 30 m. Its time resolution is 5 s, which means its observational frequency is 0.2 Hz. Specific performance indicators of the wind lidar instrument and three-dimensional ultrasonic anemometer are shown in Table 1.

The values of turbulence parameters are extremely dependent on the precision of wind speed measurements, obtained as a time series, and the presence of too many abnormal signals can lead to the inference of abnormal turbulence parameters. Therefore, it is necessary to conduct data quality control to ensure the reliability of the observed data. For the wind lidar data, an overall inspection was conducted on the wind speed measurements every 30 min every day, eliminating data with wind speed measurements deviating from the average by more than 3 standard deviations (Qiu et al., 2023). For a single wind speed profile data set, if more than 20 % of the data points were lost below 500 m, the entire profile was discarded. For the three-dimensional ultrasonic wind speed data, we calculated the average and standard deviation of the observed values within 30 min, and any observed values deviating from the average by more than 3 times the standard deviation were marked as abnormal data and assigned as missing values. We repeated the above vetting process three times. During processing, data interpolation was not performed. If the number of missing measurements exceeded 20 % within 30 min, the data were discarded. In order to eliminate wind speed errors caused by an installation tilt error of the ultrasonic anemometer, it was necessary to rotate the coordinates of the wind speed; here, we corrected the coordinate axis using the double-rotation method (Zhou et al., 2023).

The analysis of atmospheric boundary layer turbulence fluctuations, such as correlation analysis and spectral analysis, is based on the assumption that atmospheric turbulence fluctuations are stationary. The actual atmospheric turbulence field is influenced by various factors and does not have stationarity characteristics (Massman, 2006). However, if a shorter observation time is used, under relatively stable weather conditions and flat underlying surface conditions, atmospheric turbulence can be approximated as static. Turbulence stationarity requires that the main statistical variables of turbulence remain stable within the observation time; that is, the mean of the variance of the entire time period within an observation time period is roughly equal to the mean of the sum of variances of each period (Massman, 2006). In this study, data screening is conducted by determining whether the deviation between the mean variance within a 30 min observation time and the mean variance of six 5 min covariance samples within the same period is less than 0.3. Turbulence stationarity can be achieved through the stationarity coefficient, Δst, as shown in Eq. (1) (Massman, 2006):

$$\Delta\mathrm{st} = \left|\left(\sigma^5 - \sigma^{30}\right)\right| / \sigma^{30}, \quad (1)$$

where σ^{30} represents the variance of wind speed within 30 min, and σ^5 represents the average variance of six 5 min wind speed measurements made within 30 min. If $\Delta\mathrm{st} > 0.3$, the data within these 30 min are discarded. The ratio of discarded data to all data used in this study is approximately 10 %.

Table 1. Performance parameters of the ultrasonic anemometer and wind lidar instrument.

	Metrics	Technical performance requirements
Ultrasonic anemometer	Observational frequency	10 Hz
	Resolution of the wind speed	$\leq 0.1\,\mathrm{m\,s^{-1}}$
	Resolution of the wind direction	$\leq 1°$
	Range of wind speed measurements	$0–40\,\mathrm{m\,s^{-1}}$
Wind lidar	Minimum detection altitude	$\leq 30\,\mathrm{m}$
	Maximum detection altitude	3 km
	Distance resolution	30 m
	Observational frequency of the wind profile	0.2 Hz
	Resolution of the wind speed	$\leq 0.1\,\mathrm{m\,s^{-1}}$
	Resolution of the wind direction	$\leq 1°$
	Range of wind speed measurements	$0–60\,\mathrm{m\,s^{-1}}$
	Range of wind direction measurements	0–360°

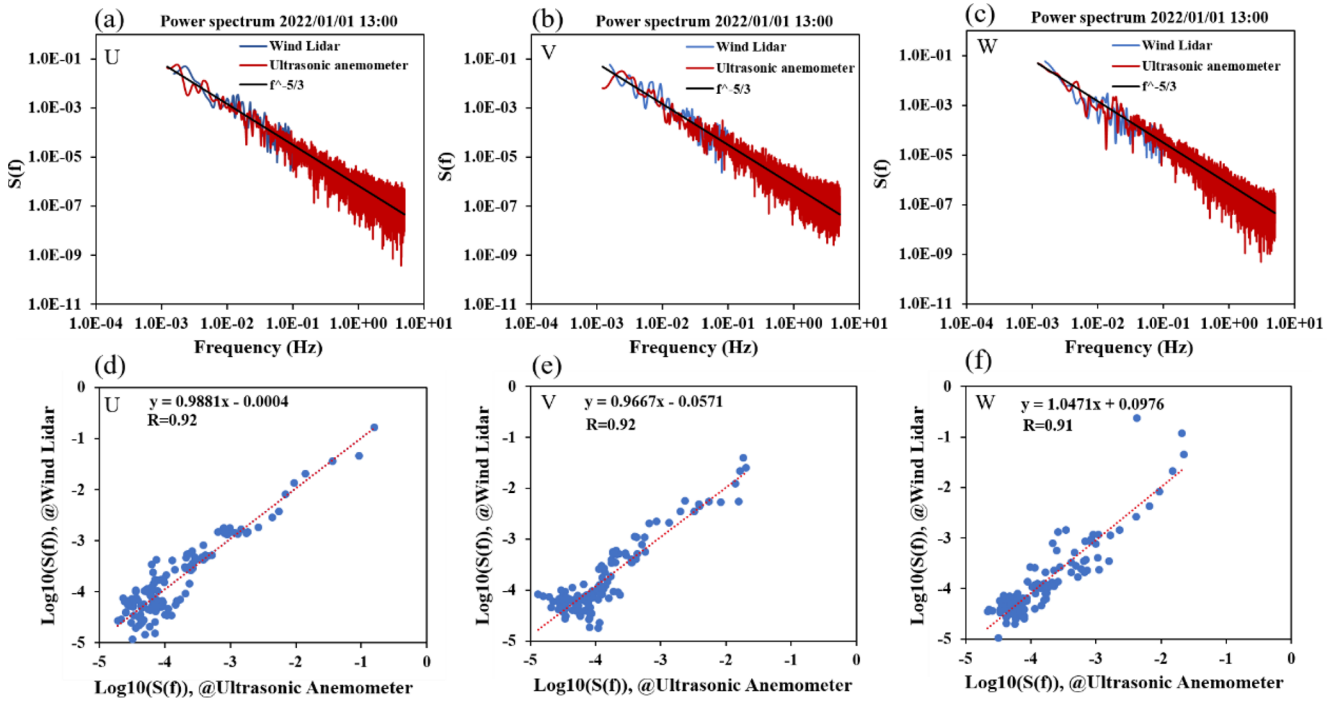

Figure 2. Comparison of the turbulence spectra obtained with the wind lidar and the ultrasonic anemometer in three directions: **(a)** U, **(b)** V, and **(c)** W, and the corresponding correlations **(d)**, **(e)**, and **(f)**.

3 Methodology

3.1 Theory

The three-dimensional wind speed measured by the wind lidar and ultrasonic anemometers can be represented as $U(z,t)$, $V(z,t)$, and $W(z,t)$, where U is the east–west direction, V is the north–south direction, W is the vertical direction, z is the height, and t is the time. Fast Fourier transform (FFT) calculations are performed on the wind speed within a certain time range at a certain height, z, to obtain the turbulence power spectrum, S, as

$$S_z(f) = \alpha \varepsilon^{-\frac{2}{3}} f^n, \tag{2}$$

where f is the frequency, α is the Kolmogorov constant, ε is the dissipation rate, and n is the power-law exponent. It is generally believed that $n = -5/3$ (Kolmogorov, 1991). In this study, it is considered a variable.

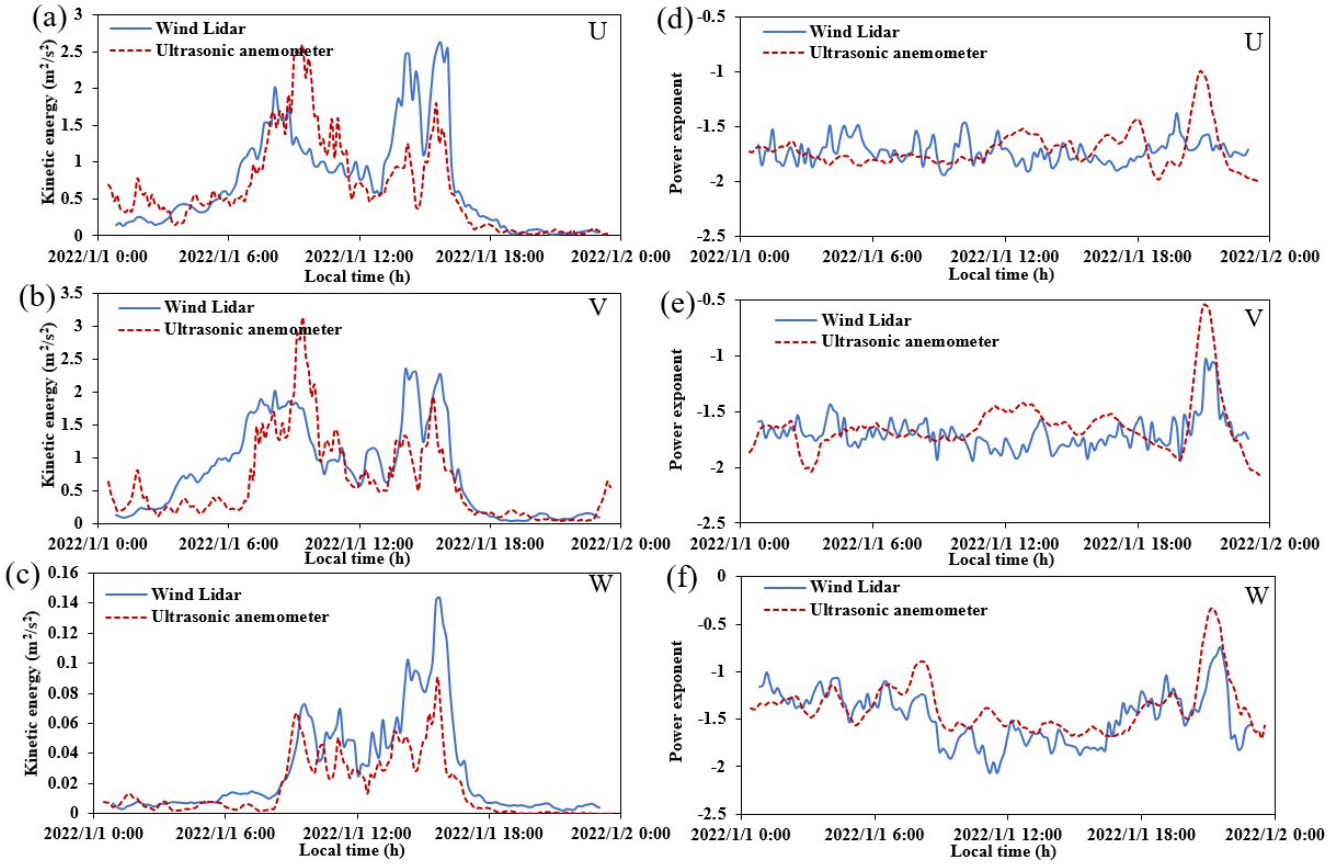

Figure 3. Comparison of the turbulent kinetic energy obtained from the wind lidar and three-dimensional ultrasonic anemometer on 1 January 2022 in the **(a)** U, **(b)** V, and **(c)** W directions and the power-law exponent distribution in the **(d)** U, **(e)** V, and **(f)** W directions.

By taking the logarithm of both sides of Eq. (2) we get

$$\log(S_z(f)) = \log\left(\alpha\varepsilon^{-\frac{2}{3}}\right) + n\log(f). \tag{3}$$

According to Eq. (3), we set

$$x = \log(f), \tag{4}$$

$$b = \log\left(\alpha\varepsilon^{-\frac{2}{3}}\right), \tag{5}$$

which are substituted into Eq. (3) to yield

$$\log(S_z(f)) = b + nx. \tag{6}$$

The slope can be obtained by performing linear fitting on x and $\log(S_z(f))$, which yields the power-law exponent n. The turbulent kinetic energy, κ, in a certain frequency range $[f_0, f_1]$ can be obtained by

$$\kappa = \sum_{f_0}^{f_1} S_z(f). \tag{7}$$

When κ and n are known, the dissipation rate can be obtained from Eq. (2). Therefore, this paper mainly discusses turbulent kinetic energy, κ, and the power-law exponent, n.

3.2 Method

Compared with traditional structure function methods that rely on the assumption of isotropy and the $-5/3$ power law, we propose a method based on spectral analysis to obtain the turbulence parameters directly. From the perspective of spectral analysis, it is possible to have a simpler and clearer understanding of atmospheric motion at different scales and types, with wider applicability and more representative significance. The scale range of vortex motion in the atmosphere is very wide, making it difficult to obtain a full-frequency spectral distribution function. Usually, based on the nature of the problem being studied, the required scale range and total sampling time of the corresponding turbulent vortices are determined. For example, when studying the contribution of thermal convection or gravitational internal waves to energy in the boundary layer atmosphere, the total sampling time cannot be less than 1 h, as detection data are required to reflect vortex motion on a timescale of 10 min (Zeng et al., 2010). When studying the contribution of turbulence to energy in the inertial subrange, the total sampling time usually takes 20 min, and the corresponding vortex scale ranges from a few seconds to several tens of seconds. In discrete FFT, 2^N

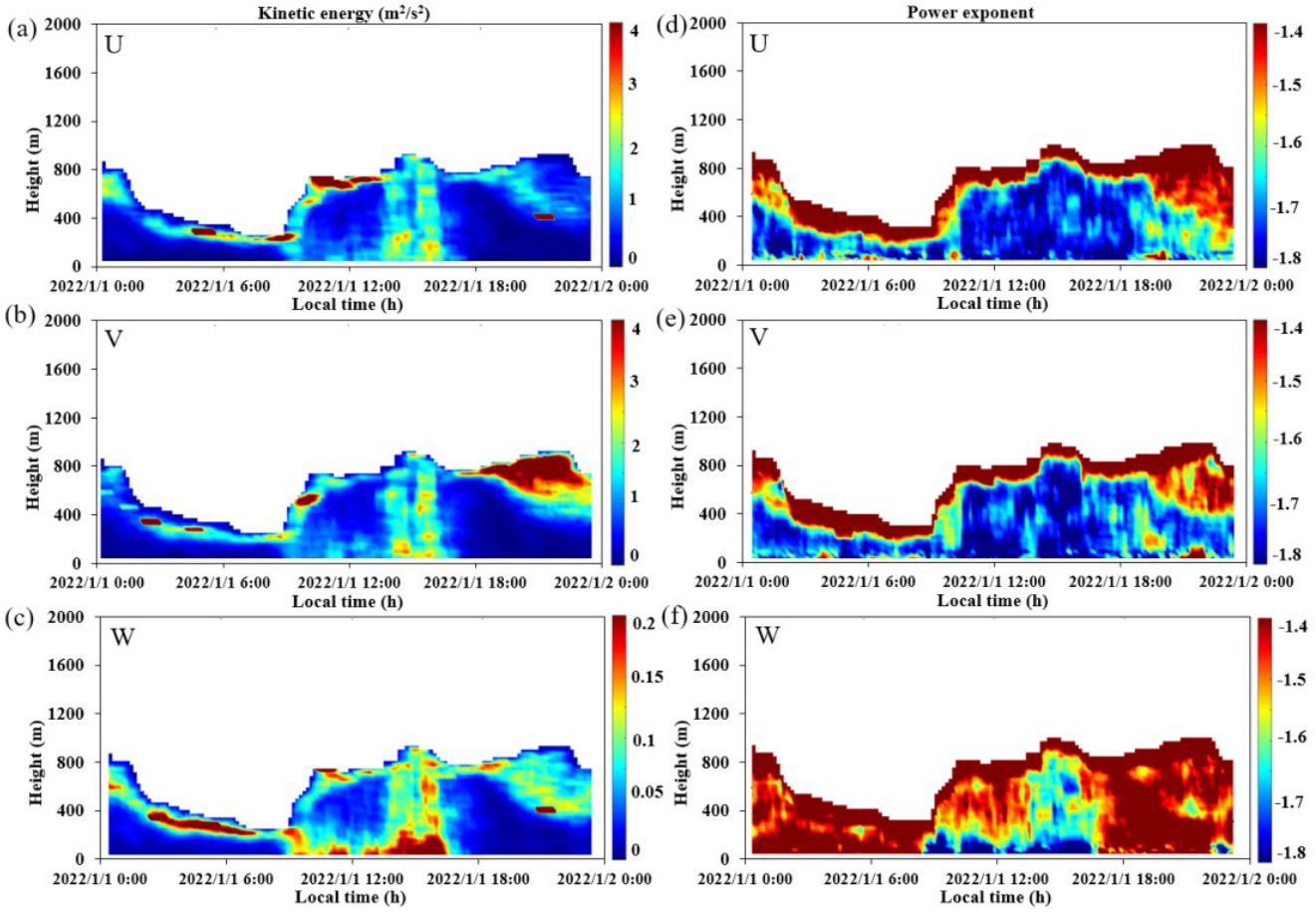

Figure 4. Temporal and spatial variations in the turbulent kinetic energy obtained by wind lidar on 1 January 2022 in the **(a)** U, **(b)** V, and **(c)** W directions and the power-law exponent distribution in the **(d)** U, **(e)** V, and **(f)** W directions.

data points are required, where N is an integer. Therefore, in this paper, we conducted FFT calculations for $2^8 \times 5$ s points (i.e., approximately 20 min) using the data obtained from the wind lidar and $2^{14} \times 0.1$ s points (i.e., approximately 27 min) for the data obtained with the ultrasonic anemometer. According to the Nyquist sampling law, the highest frequencies of turbulence spectra that can be monitored by ultrasonic anemometers and wind lidar are 5 and 0.1 Hz, respectively.

We compared the wind speed data of the wind lidar at a height of 330 m with the ultrasonic anemometer data at a height of 320 m, which are within the 30 m resolution of the wind lidar data. Figure 2a–c shows a comparison of turbulence spectra in the three directions (U, V, W) obtained with the wind lidar and ultrasonic anemometer. From the graph we can see that in all three directions the spectra have high consistency within the overlapping frequency range of $10^{-2.5}$ to 10^{-1} Hz and are in good compliance with the $-5/3$ power-law index. Figure 2d–f provides the correlation coefficients (R) corresponding to Fig. 2a–c, respectively. It can be seen that the correlation coefficients are greater than 0.9 in all three directions. This proves that wind lidar can effectively monitor the turbulence spectrum of wind within the frequency range of $10^{-2.5}$ to 10^{-1} Hz. In this study, in order to avoid differences caused by the size of the frequency domain, the frequency range was selected as the overlapping area of the two during the comparison process. Based on the method proposed in Sect. 3.1, the turbulent kinetic energy and power-law exponent within this frequency range were obtained. The structure function method assumes isotropy in atmospheric turbulence and cannot obtain power-law exponents. Using wind lidar to obtain atmospheric turbulence spectra enables the direct retrieval of not only turbulent kinetic energy, but also the power-law exponents, thus making the spectra applicable to different atmospheric conditions. We verify the applicability and accuracy of this method in the next section.

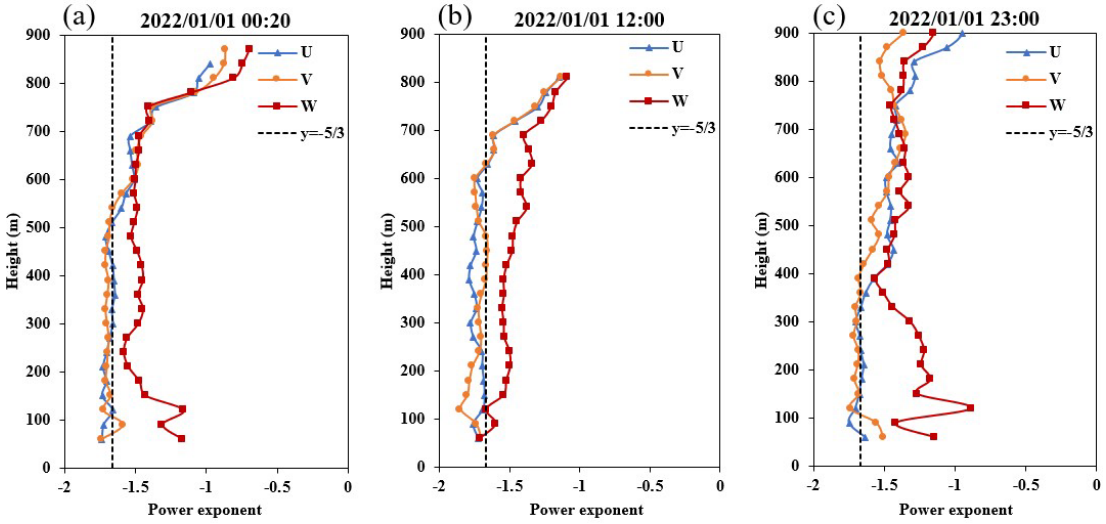

Figure 5. Power-law exponent profile of the wind speed in different directions with altitude on 1 January 2022 at **(a)** 00:20 LT, **(b)** 12:00 LT, and **(c)** 23:00 LT.

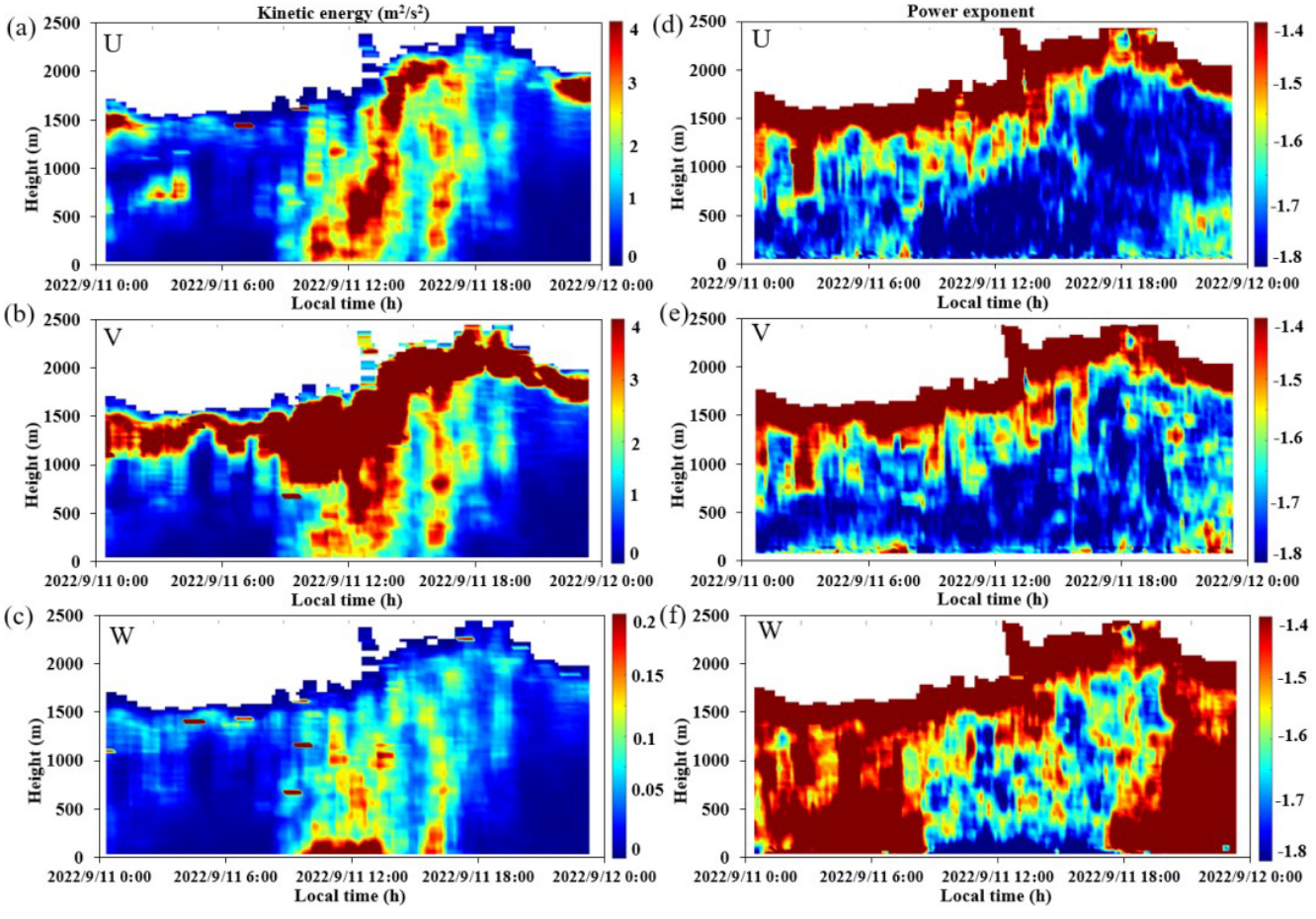

Figure 6. Temporal and spatial variations in the turbulent kinetic energy obtained by wind lidar on 11 September 2022 in the **(a)** U, **(b)** V, and **(c)** W directions and the power-law exponent distribution in the **(d)** U, **(e)** V, and **(f)** W directions.

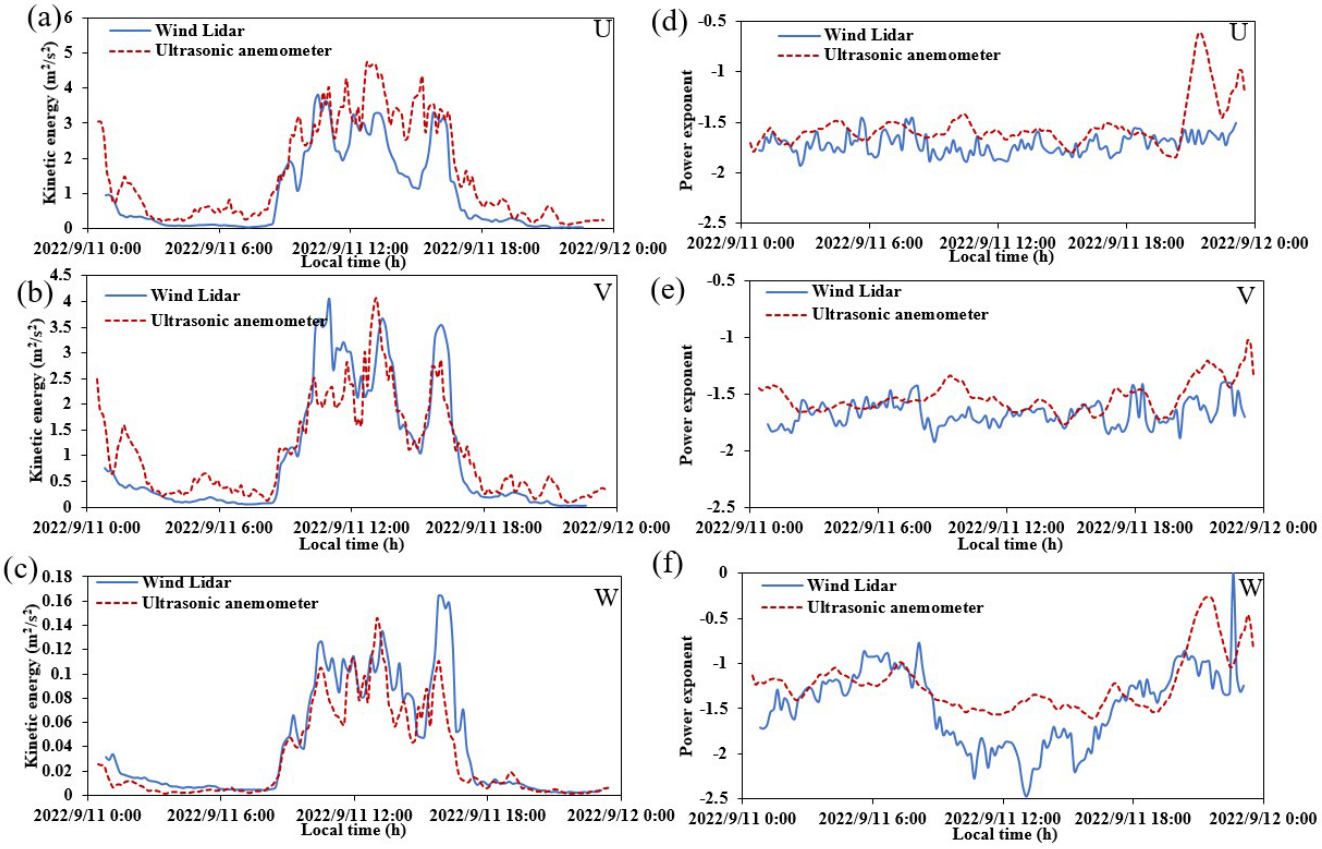

Figure 7. Comparison of the turbulent kinetic energy obtained by the wind lidar and three-dimensional ultrasonic anemometer on 11 September 2022 in the **(a)** U, **(b)** V, and **(c)** W directions and the power-law exponent distribution in the **(d)** U, **(e)** V, and **(f)** W directions.

4 Results and discussion

4.1 Detection performance under weak convection

Using the method proposed in Sect. 3.2, based on the high-resolution wind lidar data, we obtained the kinetic energy and power-law exponent at different heights; here a height of 330 m was selected as an example, and the results are compared with those obtained with the three-dimensional ultrasonic anemometer. As mentioned in Sect. 3.2, in all subsequent comparisons, the time resolutions of the wind lidar and ultrasonic anemometer data were maintained at 20 and 27 min, respectively. Figure 3 shows a comparison of the turbulent kinetic energy obtained by wind lidar and the three-dimensional ultrasonic anemometer on 1 January 2022. The weather on that date was clear and cloudless, with an average temperature of 14 °C. The main wind direction was easterly, with an average horizontal wind speed of $\sim 3\,\mathrm{m\,s^{-1}}$. From the graph, it can be seen that the results of both in all three directions are relatively consistent, verifying the accuracy of wind lidar in monitoring the vertical characteristics of atmospheric turbulence.

On this basis, we produced spatiotemporal distribution maps of the turbulent kinetic energy and power-law exponent, as shown in Fig. 4, where panels Fig. 4a–c correspond to wind speed components U, V, and W, respectively. In our model we do not assume the $-5/3$ power law but instead allow it to be a free parameter. Thus, we also present a spatiotemporal distribution map of the power-law exponent of the inertial subrange in the three directions in Fig. 4d–f. We can observe the vertical structure and characteristics of turbulence in Fig. 4. From Fig. 4a–c, it can be seen that the kinetic energy in the U and V directions was relatively consistent near the ground surface, but significant differences are seen at high altitudes, such as between 18:00 and 24:00 local time (LT). The turbulent kinetic energy in the W direction was relatively small because, compared to the horizontal wind speed, the vertical wind speed was relatively small. From Fig. 4d–f it can be seen that the power-law exponent in the U and V directions was relatively consistent most of the time, which is more in line with isotropic theory. However, at high altitudes at night there were significant differences, where the power-law exponent in the vertical direction (W) showed a phenomenon of being high at night and low during the day. This is because the vertical wind speed is mainly driven by ground heating radiation during the day. At night, due to the weakening of solar radiation, the kinetic energy in the verti-

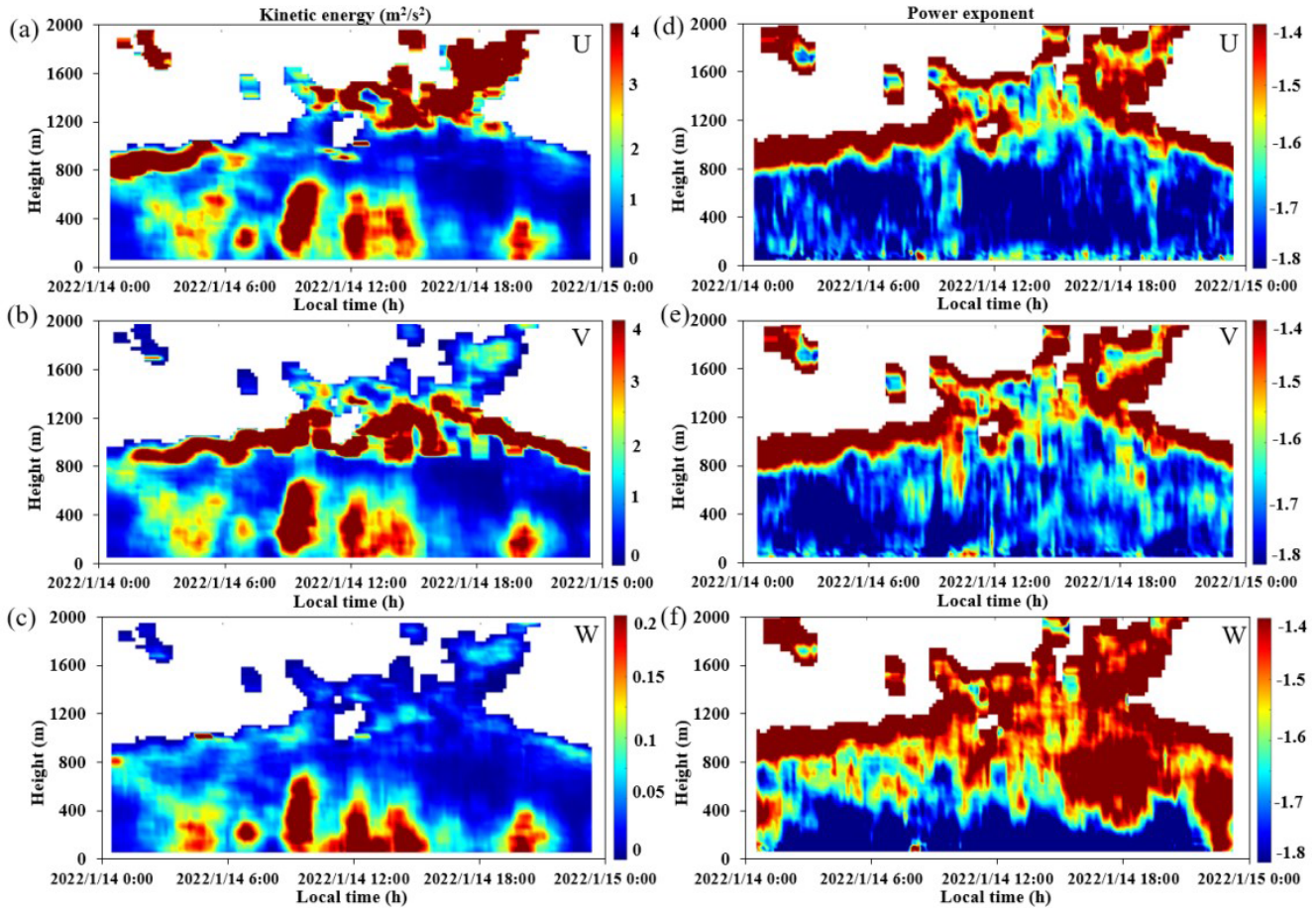

Figure 8. Temporal and spatial variations in the turbulent kinetic energy obtained by wind lidar on 14 January 2022 in the **(a)** U, **(b)** V, and **(c)** W directions and the power-law exponent distribution in the **(d)** U, **(e)** V, and **(f)** W directions.

cal direction is suppressed, and the power-law exponent increases.

Furthermore, we present the derived power-law exponent profile in the three different directions at different local times on 1 January 2022 in Fig. 5. From the graph it can be seen that the power-law exponent changed similarly in the U and V directions with height. From Fig. 5a it can be seen that at altitudes $\sim$600–800 m, the turbulence in all three directions conformed to the assumptions of homogeneity and isotropy, while at other altitudes, the turbulence in all three directions was anisotropic. As the height increased, the power-law exponents in all three directions increased, corresponding to the power-law exponent distributions shown in Fig. 4d–f, where there was a layer with a higher power-law exponent, indicating the presence of kinetic energy suppression at the top of the boundary layer. Both Fig. 4 and Fig. 5 intuitively and clearly reflect that the atmosphere was not isotropic and the power-law exponent was not entirely $-5/3$, indicating that the atmospheric turbulence parameters obtained by the spectral analysis method proposed in this study are more in line with the actual atmospheric conditions and therefore have good accuracy.

4.2 Detection performance under strong convection

To verify the effectiveness of the proposed method under different weather conditions, Fig. 6 shows the spatiotemporal variations in the turbulent kinetic energy and the power-law exponent on 11 September 2022. The weather on this day was clear and cloudless, with an average temperature of 27 °C. The main wind direction was southwest, with an average wind speed of about $\sim 3\,\mathrm{m\,s^{-1}}$. From the graph it can be seen that the convection was stronger on this day, with a boundary layer height of about 2000 m. The turbulent kinetic energy in the U and V directions exhibited significant differences at different altitudes. The power-law exponent was relatively consistent most of the time, more in line with the assumption of isotropy, but exhibited significant differences near the ground at night. This may be due to daytime heating radiation resulting in more homogeneous atmospheric mixing, which is more in line with the isotropic hypothesis. The power-law exponent in the vertical direction (W) was also

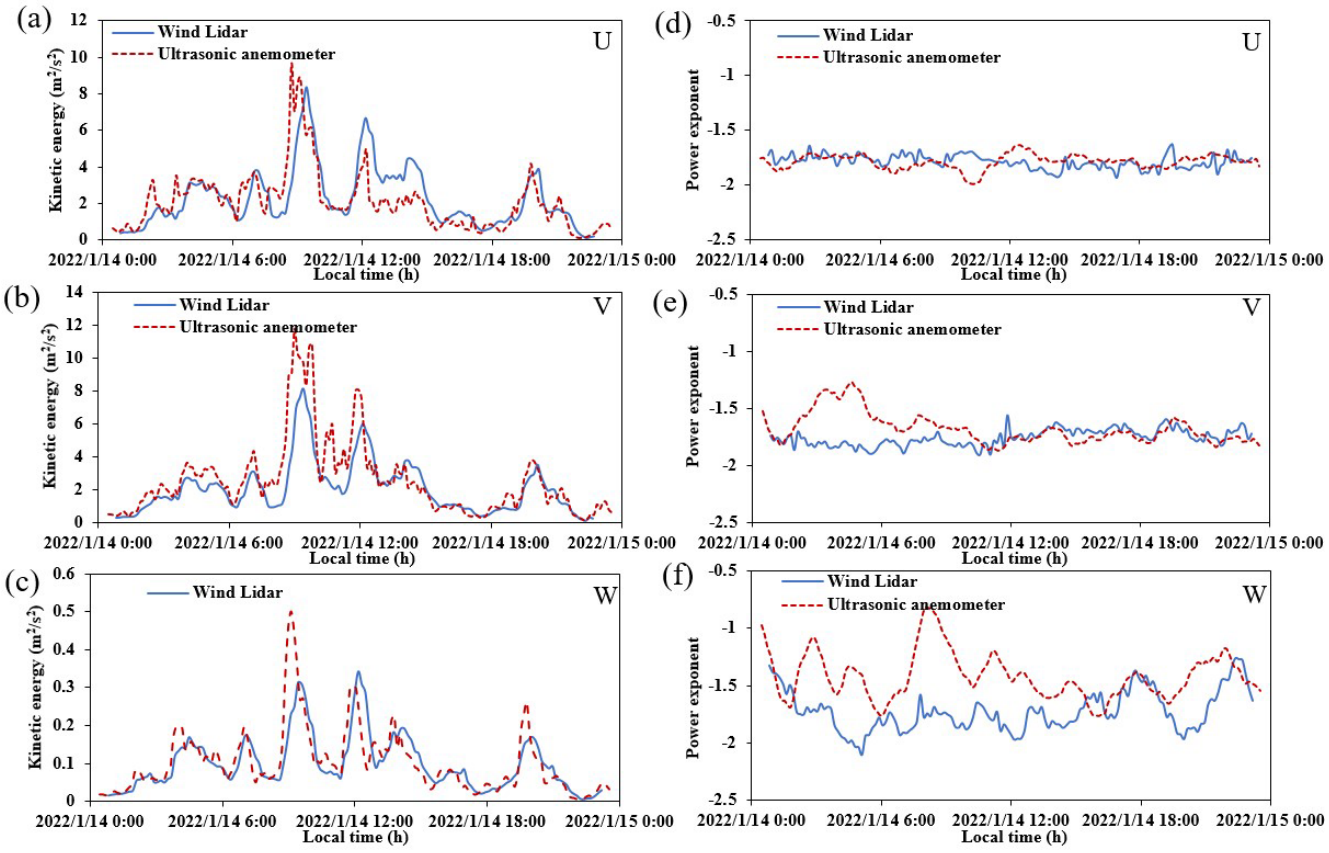

Figure 9. Comparison of turbulent kinetic energy obtained by the wind lidar and three-dimensional ultrasonic anemometer on 14 January 2022 in the **(a)** U, **(b)** V, and **(c)** W directions and the power-law exponent distribution in the **(d)** U, **(e)** V, and **(f)** W directions.

high at night and low during the day. Similarly, the turbulent kinetic energy and power-law exponent at a height of 330 m were selected and compared with the results from the three-dimensional ultrasonic anemometer, as shown in Fig. 7. The installation of the ultrasonic anemometer on the north side of the gradient tower was likely affected by wind obstruction caused by the tower, with the effect being most significant from 00:00 to 06:00 LT. We infer this obstruction effect based on nighttime data collected by the ultrasonic anemometer, such as near midnight, where the measured turbulent kinetic energy was found to be close to its intensity measured during the day. From the graph, it can be seen that the results of both in all three directions are relatively consistent, further verifying the accuracy and applicability of wind lidar in monitoring the vertical characteristics of atmospheric turbulence.

4.3 Detection performance in cloudy weather

Figure 8 shows the spatiotemporal variations in the turbulent kinetic energy and power-law exponent on 14 January 2022. On that day, the weather was cloudy with an average temperature of 13 °C. The main wind direction was easterly, with an average wind speed of 6 m s^{-1}. Similar to the previous results, the power-law exponent in the U and V directions was relatively consistent, in line with the assumption of isotropy. The power-law exponent in the vertical direction (W) was mainly affected by surface temperature radiation. Due to the cover of clouds during the day, the difference in the surface temperature radiation between day and night was not significant, so the phenomenon of a higher power-law exponent at night and a lower exponent during the day was not obvious. Figure 9 shows a comparison of the turbulent kinetic energy obtained by wind lidar and the three-dimensional ultrasonic anemometer on the same date. From Fig. 9a–c it can be seen that the turbulent kinetic energy peaked multiple times, and the results from the two methods have high consistency under complex weather conditions. In Fig. 9d and e, the power-law exponents of the two in the U and V directions are also relatively consistent. This means that the method proposed has good performance in predicting the turbulent kinetic energy and power-law exponent in these directions in cloudy weather. In Fig. 9f, there is a significant difference in the power-law exponent between the two in the W direction. Because it was a cloudy day, the vertical wind speed on that day was relatively low, about 0.1 m s^{-1}. We attribute this difference to the different measurement principles of the different instruments, namely that the ultrasonic anemometer requires

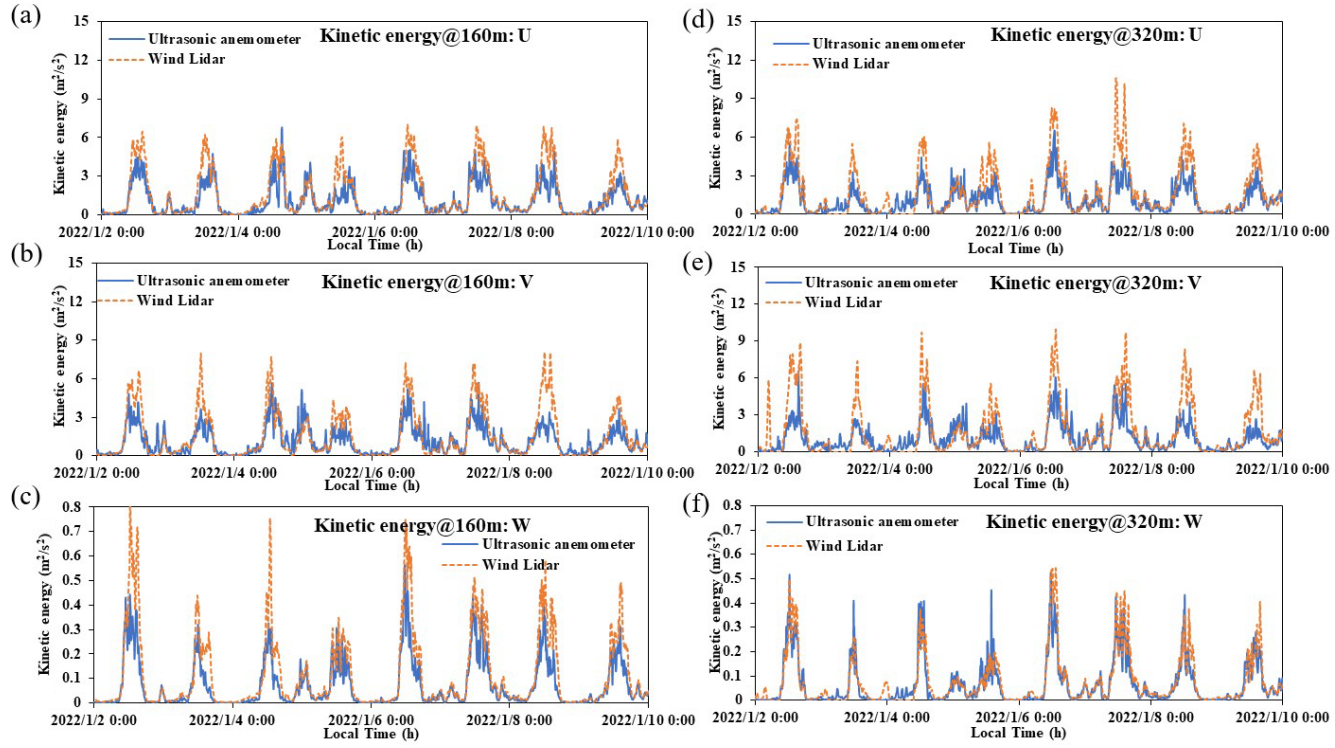

Figure 10. Comparison of the turbulent kinetic energy obtained from the wind lidar and three-dimensional ultrasonic anemometer from 2 to 10 January 2022 in the U, V, and W directions at the heights of 160 m **(a–c)** and 320 m **(d–f)**.

a minimum wind speed ($\sim 0.01\,\mathrm{m\,s^{-1}}$) to start making measurements, whereas the wind lidar has no such dependency. This indicates that the method proposed in this study can be utilized under different weather conditions and has high applicability.

4.4 Continuous long-term verification

Figure 10 shows a comparison of the long-term, continuous turbulent kinetic energy obtained from the wind lidar and three-dimensional ultrasonic anemometer from 2 to 10 January 2022, where Fig. 10a–c and d–f correspond to the heights of 160 and 320 m, respectively. From the graph, we can see that the results of the wind lidar and ultrasonic anemometer are relatively consistent at the different heights. Figure 11 shows the correlation of the turbulent kinetic energy measured by the wind lidar and ultrasonic anemometer in all three directions, where Fig. 10a–c and d–f correspond to the same heights of 160 and 320 m, respectively, with sample sizes (N) all greater than 2800. From the figure it can be seen that the results are relatively linear, with correlation coefficients greater than 0.9, and the slope of the fitting line approaches 1 in the U, V, and W directions. Compared to the U and V components, the consistency of the comparison results in the W direction is the highest. This is because under different horizontal wind directions, the results of the U and V components are more susceptible to interference from the gradient tower itself, while the vertical wind speed (W) is not affected by this, thus yielding better results. This comparison of the continuous results indicates that the proposed method has a high applicability and accuracy.

5 Conclusion

We proposed a method for directly measuring atmospheric turbulence parameters using coherent Doppler wind lidar from the perspective of spectral analysis without assuming isotropy and the $-5/3$ power law. The method can intuitively reflect the vertical characteristics of atmospheric turbulence. In our method, the power-law index is left as a free parameter, and based on our results we have presented, for the first time, a power-law exponent spatiotemporal distribution map for the inertial subrange is provided. The results indicate that the atmosphere does not always conform to the assumption of isotropy and the $-5/3$ power law, which verifies that the proposed method of directly obtaining atmospheric turbulence parameters from spectral analysis is more in line with the actual atmospheric conditions and has good accuracy. The obtained turbulent kinetic energy and power-law exponent were compared with the results obtained with ultrasonic anemometers for different weather conditions and over a long period (1 month). The results of the three wind speed components (U, V, and W) showed good consistency,

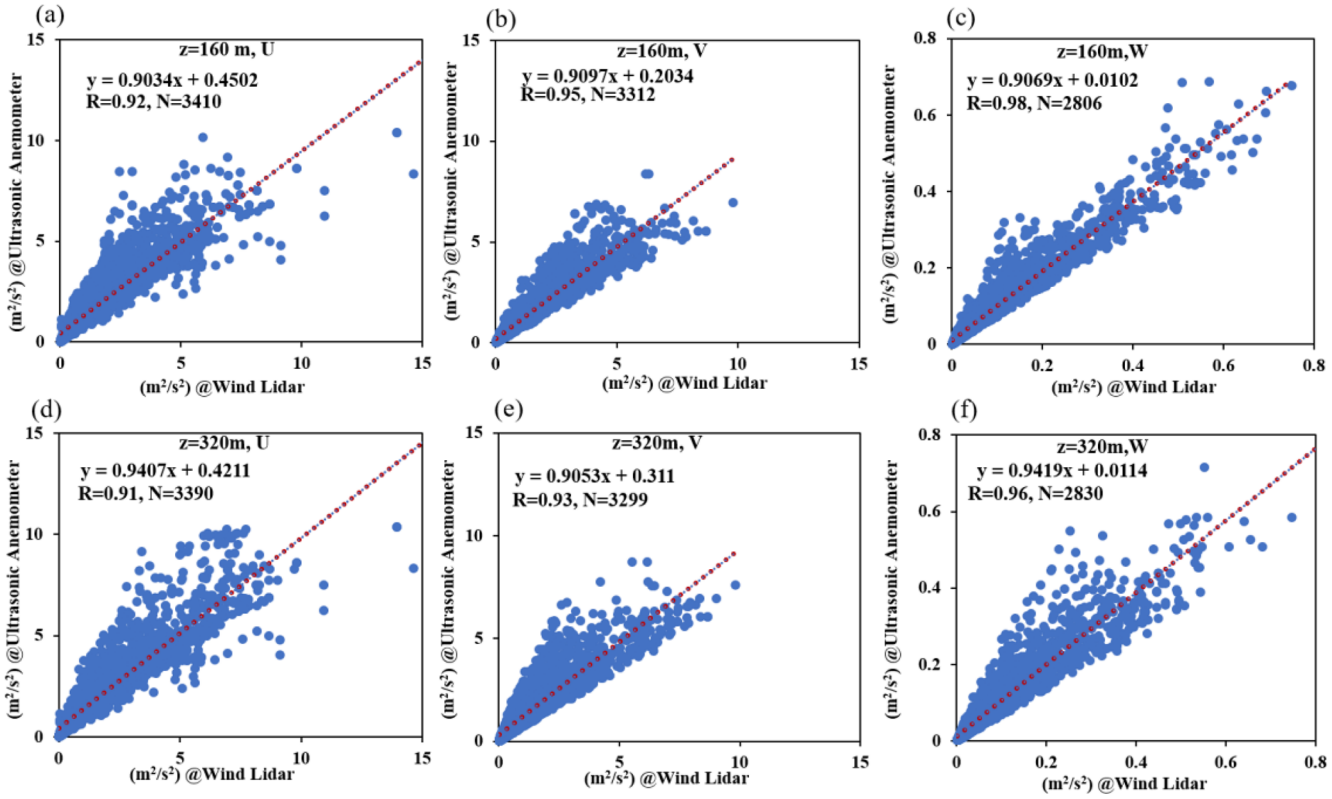

Figure 11. Correlation between the turbulent kinetic energy obtained with the wind lidar and three-dimensional ultrasonic anemometer in the U, V, and W directions at the heights of 160 m **(a–c)** and 320 m **(d–f)**.

with correlations reaching 0.91, 0.93, and 0.96, respectively. In complex weather conditions, there was still a high degree of consistency between the two results, indicating that the method proposed in this study has high applicability and accuracy. However, the proposed method has some limitations. First, the method is based on a spectral analysis that requires the atmospheric turbulence fluctuations to be stable. Next, wind lidar cannot operate during heavy rainfall or snowy weather conditions, so it cannot be guaranteed to be applicable at all times. In addition, due to the maximum observation frequency of 0.2 Hz for wind lidar, the observed scale range of vortex motion is limited. However, the results of this study also indicate that in the inertial subrange, turbulence spectra outside the frequency of 0.2 Hz can be obtained through fitting and extrapolation. Compared with traditional structure function methods that rely on isotropic assumptions and the $-5/3$ power law, the proposed method has higher applicability and accuracy with fewer assumptions. It can obtain the spatiotemporal distributions of atmospheric turbulence parameters, which have important significance in weather prediction, meteorological disasters, and forecasting.

Data availability. The data are available from the authors upon request.

Author contributions. Conceptualization, JX; methodology, JX; software, JX; validation, CL; formal analysis, JX; investigation, XL; resources, CL; data curation, LZ; writing – original draft preparation, JX; writing – review and editing, HY and NZ; visualization, XL; supervision, HY and NZ; project administration, HY and NZ; funding acquisition, HY and NZ.

Competing interests. The contact author has declared that none of the authors has any competing interests.

Disclaimer. Publisher's note: Copernicus Publications remains neutral with regard to jurisdictional claims made in the text, published maps, institutional affiliations, or any other geographical representation in this paper. While Copernicus Publications makes every effort to include appropriate place names, the final responsibility lies with the authors.

Acknowledgements. We thank Shenzhen Darsunlaser Technology Co., Ltd.

Financial support. This work was supported by the National Key R&D Program of China (grant no. 2019YFE0124800), the Special Project for Sustainable Development of Shenzhen (grant

no. KCXFZ20201221173412035), the National Natural Science Foundation of China (NSFC; grant nos. 42275065 and U2342221), the Guangdong Province Science and Technology Department project (grant no. 2021B1212050024), the scientific research projects of the Guangdong Provincial Meteorological Bureau (grant no. GRMC2020M29), and the Science and Technology Innovation Team Plan of the Guangdong Meteorological Bureau (grant no. GRMCTD202003).

Review statement. This paper was edited by Yuanjian Yang and reviewed by Hao Yang and two anonymous referees.

References

Banakh, V. and Smalikho, I.: Coherent Doppler Wind Lidars in a Turbulent Atmosphere, Artech House Publishers, Boston, London, ISBN 9781608076673, 2013.

Banakh, V. A., Smalikho, I. N., Falits, A. V., and Sherstobitov, A. M.: Estimating the Parameters of Wind Turbulence from Spectra of Radial Velocity Measured by a Pulsed Doppler Lidar, Remote Sens., 13, 2071, https://doi.org/10.3390/rs13112071, 2021.

Bonin, T. A., Newman, J. F., Klein, P. M., Chilson, P. B., and Wharton, S.: Improvement of vertical velocity statistics measured by a Doppler lidar through comparison with sonic anemometer observations, Atmos. Meas. Tech., 9, 5833–5852, https://doi.org/10.5194/amt-9-5833-2016, 2016.

Bonin, T. A., Choukulkar, A., Brewer, W. A., Sandberg, S. P., Weickmann, A. M., Pichugina, Y. L., Banta, R. M., Oncley, S. P., and Wolfe, D. E.: Evaluation of turbulence measurement techniques from a single Doppler lidar, Atmos. Meas. Tech., 10, 3021–3039, https://doi.org/10.5194/amt-10-3021-2017, 2017.

Branlard, E., Pedersen, A. T., Mann, J., Angelou, N., Fischer, A., Mikkelsen, T., Harris, M., Slinger, C., and Montes, B. F.: Retrieving wind statistics from average spectrum of continuous-wave lidar, Atmos. Meas. Tech., 6, 1673–1683, https://doi.org/10.5194/amt-6-1673-2013, 2013.

Byzova, N. L., Ivanov, V. N., and Garger, E. K.: Turbulence in Atmospheric Boundary Layer, Gidrometeoizdat, Leningrad, ISBN 9785286001514, 1989.

Chan, P. W. and Lee, Y. F.: Application of Short-Range Lidar in Wind Shear Alerting, J. Atmos. Ocean. Techn., 29, 207–220, https://doi.org/10.1175/JTECH-D-11-00086.1, 2012.

Chellali, F., Khellaf, A., and Belouchrani, A.: Application of time-frequency representation in the study of the cyclical behavior of wind speed in Algeria: wavelet transform, Stoch. Env. Res. Risk A., 24, 1233–1239, https://doi.org/10.1007/s00477-010-0388-x, 2010.

Choukulkar, A., Brewer, W. A., Sandberg, S. P., Weickmann, A., Bonin, T. A., Hardesty, R. M., Lundquist, J. K., Delgado, R., Iungo, G. V., Ashton, R., Debnath, M., Bianco, L., Wilczak, J. M., Oncley, S., and Wolfe, D.: Evaluation of single and multiple Doppler lidar techniques to measure complex flow during the XPIA field campaign, Atmos. Meas. Tech., 10, 247–264, https://doi.org/10.5194/amt-10-247-2017, 2017.

Frehlich, R. and Cornman, L.: Estimating spatial velocity statistics with coherent Doppler lidar, J. Atmos. Ocean. Techn., 19, 355–366, https://doi.org/10.1175/1520-0426-19.3.355, 2002.

Frehlich, R. and Kelley, N.: Measurements of Wind and Turbulence Profiles With Scanning Doppler Lidar for Wind Energy Applications, IEEE J. Sel. Top. Appl., 1, 42–47, https://doi.org/10.1109/JSTARS.2008.2001758, 2008.

Gottschall, J. and Peinke, J.: How to improve the estimation of power curves for wind turbines, Environ. Res. Lett., 3, 015005, https://doi.org/10.1088/1748-9326/3/1/015005, 2008.

Jin, X., Song, X. Q., Yang, Y. W., Wang, M. A., Shao, S. Y., and Zheng, H. T.: Estimation of turbulence parameters in the atmospheric boundary layer of the Bohai Sea, China, by coherent Doppler lidar and mesoscale model, Opt. Express, 30, 13263–13277, https://doi.org/10.1364/OE.455079, 2022.

Kolmogorov, A. N.: Energy dissipation in locally isotropic turbulence, Dokl. Akad. Nauk SSSR, 32, 19–21, 1941.

Kolmogorov, A. N.: Dissipation of energy in the locally isotropic turbulence, P. Roy. Soc. Lond. A Mat., 434A, 15–17, 1991.

Mann, J., Peña, A., Bingöl, F., Wagner, R., and Courtney, M. S.: Lidar Scanning of Momentum Flux in and above the Atmospheric Surface Layer, J. Atmos. Ocean. Techn., 27, 959–976, https://doi.org/10.1175/2010JTECHA1389.1, 2010.

Massman, W.: Handbook of Micrometeorology: A Guide for Surface Flux Measurement and Analysis, Kluwer Academic, Boston, ISBN 9781402022647, 2006.

O'Connor, E. J., Illingworth, A. J., Brooks, I. M., Westbrook, C. D., Hogan, R. J., Davies, F., and Brooks, B. J.: A Method for Estimating the Turbulent Kinetic Energy Dissipation Rate from a Vertically Pointing Doppler Lidar, and Independent Evaluation from Balloon-Borne In Situ Measurements, J. Atmos. Ocean. Techn., 27, 1652–1664, https://doi.org/10.1175/2010JTECHA1455.1, 2010.

Panofsky, H. A., Larko, D., Lipschutz, R., Stone, G., Bradley, E. F., Bowen, A. J., and Hojstrup, J.: Spectra of velocity components over complex terrain, Q. J. Roy. Meteor. Soc., 108, 215–230, https://doi.org/10.1256/smsqj.45512, 1982.

Qiu, Z. X., Xian, J. H., Yang, Y. X., Lu, C., Yang, H. L., Hu, Y. Y., Sun, J. Q., and Zhang, C. S.: Characteristics of Coastal Low-Level Jets in the Boundary Layer of the Pearl River Estuary, Journal of Marine Science and Engineering, 11, 1128, https://doi.org/10.3390/jmse11061128, 2023.

Sathe, A. and Mann, J.: A review of turbulence measurements using ground-based wind lidars, Atmos. Meas. Tech., 6, 3147–3167, https://doi.org/10.5194/amt-6-3147-2013, 2013.

Smalikho, I., Köpp, F., and Rahm, S.: Measurement of atmospheric turbulence by 2-μm Doppler lidar, J. Atmos. Ocean. Techn., 22, 1733–1747, https://doi.org/10.1175/JTECH1815.1, 2005.

Smalikho, I. N. and Banakh, V. A.: Measurements of wind turbulence parameters by a conically scanning coherent Doppler lidar in the atmospheric boundary layer, Atmos. Meas. Tech., 10, 4191–4208, https://doi.org/10.5194/amt-10-4191-2017, 2017.

Stull, R. B.: An Introduction to Boundary Layer Meteorology, Springer Netherlands, ISBN 9789027727695, 1988.

Wang, X. Y., Dai, G. Y., Wu, S. H., Zhu, P. Z., Li, Z. W., Song, X. Q., Zhang, S. P., Xu, J., Yin, J. P., Qin, S. G., and Wang, X. T.: Classification of Turbulent Mixing Driven Sources in Marine Atmospheric Boundary Layer With Use of Shipborne Coherent Doppler Lidar Observations, J. Geophys. Res.-Atmos., 128, e2023JD038918, https://doi.org/10.1029/2023JD038918, 2023.

Zeng, Q. C., Cheng, X. L., Hu, F., and Peng, Z.: Gustiness and coherent structure of strong winds and their role in

dust emission and entrainment, Adv. Atmos. Sci., 27, 1–13, https://doi.org/10.1007/s00376-009-8207-3, 2010.

Zhai, X. C., Wu, S. H., and Liu, B. Y.: Doppler lidar investigation of wind turbine wake characteristics and atmospheric turbulence under different surface roughness, Opt. Express, 25, A515–A529, https://doi.org/10.1364/OE.25.00A515, 2017.

Zhou, Q. J., Li, L., Chan, P. W., Cheng, X. L., Lan, C. X., Su, J. C., He, Y. Q., and Yang, H. L.: Observational Study of Wind Velocity and Structures during Supertyphoons and Convective Gales over Land Based on a 356-m-High Meteorological Gradient Tower, J. Appl. Meteorol. Clim., 62, 103–118, https://doi.org/10.1175/JAMC-D-22-0013.1, 2023.